Materials Research Proceedings 41 (2024) 1935-1944 https://doi.org/10.21741/9781644903131-214

Fatigue strength of Ti6Al4V titanium alloy machined under flood and cryogenic conditions

STRAMARE Andrea[1,a], BERTOLINI Rachele[1,b*], BRUSCHI Stefania[1,c], GHIOTTI Andrea[1,d] and CAMPAGNOLO Alberto[1,e]

[1]Department of Industrial Engineering, University of Padova, Via Venezia 1, 35131 Padova, Italy

[a]andrea.stramare@unipd.it, [b]rachele.bertolini@unipd.it, [c]stefania.bruschi@unipd.it, [d]andrea.ghiotti@unipd.it, [e]alberto.campagnolo@unipd.it

Keywords: Ti6Al4V, Cryogenic Machining, Surface Integrity, Fatigue Strength

Abstract. Ti6Al4V titanium alloy wrought round bars characterized by a fine equiaxed microstructure were machined using two different lubrication strategies, namely traditional water-based cutting fluid and liquid nitrogen. Surface integrity after machining was assessed in terms of (i) sub-surface severe plastic deformation layer, (ii) surface topography, and (iii) residual axial stresses as a function of the distance from the machined surface. Finally, the machined specimens were subjected to fatigue tests on a four-point rotating bending machine. For the two sets of specimens, the Wöhler curves were derived to determine their fatigue strength using the modified staircase method. No remarkable difference in terms of surface topography was found between the flood and cryogenic machined specimens, but the latter were characterized by higher and deeper compressive residual stresses and higher severe plastic deformation layer beneath the machined surface. Despite that, it is shown that the fatigue limit of the flood and cryogenic machined specimens is very similar, as well as crack initiation sites have the same location. An explanation of that can be found in the very fine microstructure of the as-received material, which prevails over the other characteristics induced by any machining strategy.

Introduction

Ti6Al4V titanium alloy is widely used in different fields, thanks to its high strength-to-weight ratio, corrosion resistance, and biocompatibility which make it suitable for aerospace and biomedical applications [1]. The last years have seen the ever-increasing use of additive manufacturing (AM) technologies to manufacture parts made of Ti6Al4V, thanks to the advantages AM can offer, mainly in terms of “complexity for free” fabrication. Nevertheless, conventional processing routes including hot forging of the wrought alloy followed by machining operations still remain the most reliable ones since they ensure the absence of internal defects like porosities characterizing AM parts, and, at the same time, offer the possibility of a precise tailoring of the part microstructure through adequate thermo-mechanical treatments [2]. Microstructure plays indeed a crucial role in assessing the part in-service characteristics.

When referring to fatigue life, the final machining steps of the processing route have the highest impact, as they may induce significant variations in the part surface integrity. It is well-known that the higher the latter the higher the part fatigue resistance, which has driven the development of innovative cutting technologies capable of assuring enhanced surface properties. Among these technologies, cryogenic machining making use of liquid nitrogen as cooling medium has recently emerged as a suitable strategy to improve the surface finish and increase surface hardness over conventional flood machining [3]. While the advantages offered by cryogenic machining in increasing the part surface integrity are well-established, few studies are available in literature that assess its impact on the part fatigue resistance. In [4] the fatigue life of a wrought Ti6Al4V with an equiaxed structure was found to be higher when machined under cryogenic cooling conditions compared to dry and conventionally lubricated conditions as a consequence of grain refinement

under the machined surface and improved surface finish induced by the application of liquid nitrogen. Nevertheless, the latter study makes use of a pull-pull fatigue test approach that may not be suitable to evaluate the effect of the machining-affected sub-surface layer on the material fatigue resistance. The fatigue life of Ti6Al4V samples fabricated through the AM technology known as laser powder bed fusion (LPBF) and then cryogenic machined was evaluated in [5] under a rotating bending loading. There was proved a substantial increase in fatigue strength of the cryogenic machined samples compared to the ones machined under conventional flooding conditions, which was ascribed to the much more significant residual compressive layer induced by the cryogenic cutting as well as the development of a hard and harmonic microstructure [6].

Nevertheless, the effect of cryogenic machining on the Ti6Al4V fatigue properties needs to be further investigated, especially in the case of the wrought alloy. In this framework, the paper aims to evaluate the fatigue strength of the wrought Ti6Al4V after flood and cryogenic machining, correlating it to the surface integrity induced by the specific cutting operation.

Materials and methods

The fatigue specimens were machined from round bars of 12 mm diameter and 3200 mm length of wrought Ti6Al4V titanium alloy, purchased in an annealed state. The microstructure of the wrought Ti6Al4V in the as-received condition was evaluated using optical microscopy (OM) using a Leica™ DMRE microscope. The material was prepared using a metallographic procedure, including hot mounting in a thermosetting resin, grinding with silicon carbide abrasive papers, fine polishing using a mapped cloth in a slurry of 2/3, in volume, 0.2 μm alkaline fumed silica suspension and 1/3 of 30% H_2O_2, cleaning in an ultrasonic bath, and final etching making use of the Kroll's etchant (10 ml HF, 5 ml HNO_3, 85 ml H_2O). Fig. 1 shows the as-received microstructure of the wrought Ti6Al4V, which consists of an equiaxed α phase and intergranular β phase, with an average grain size of 2.6 ± 0.3 μm calculated through image analysis with the ImageJ™ software. It is worth noting that the as-received microstructure is very fine, which should correspond to high fatigue strength as a consequence of the increased resistance to crack initiation provided by fine microstructural features [7]. The wrought Ti6Al4V micro-hardness in the as-received condition was measured by making use of a Leitz™ Durimet Miniload hardness tester with a load of 100 gr for 30 s of indentation duration. The average hardness resulted in 291.6 HV ± 16.3. Finally, the ultimate tensile strength (UTS) certified by the supplier was 963 MPa.

Fatigue specimens with an hourglass shape (geometry in Fig. 2a) were machined from the wrought Ti6Al4V bars. The specimen dimensions were chosen to ensure its failure within the medium-to-high-cycle fatigue range, that is between 10^4 and $2*10^6$ cycles. The specimen machining was carried out on a Mori Seiki™ NL 1500 CNC lathe adopting two lubricating-cooling conditions, namely conventional flood with a water-based cutting fluid containing 5% semi-synthetic oil, and cryogenic cooling with liquid nitrogen sprayed towards the tool rake and flank faces through 0.9 mm diameter copper nozzles. A total of 30 specimens (15 flood and 15 cryogenic) were machined. Fig. 2b shows the machining set-up when applying cryogenic cooling. A Sandvik Coromant™ VCET 1103 01-UM 1115 cutting tool was chosen as suitable for machining difficult-to-cut metal alloys, adopting a cutting speed of 45 m/min and feed of 0.03 mm/rev as suggested by the tool manufacturer. The final turning step to obtain the geometry of the specimen gauge length was carried out using a depth of cut of 0.25 mm.

The machined surface finish was analyzed using the Sensofar Metrology™ S-Neox 3D optical profiler equipped with Nikon™ TU Plan Fluor-EPI 20x confocal objective. The surface finish was assessed according to the ISO 25178 standard, applying a 2.5 μm S-filter and 0.25 μm L-filter.

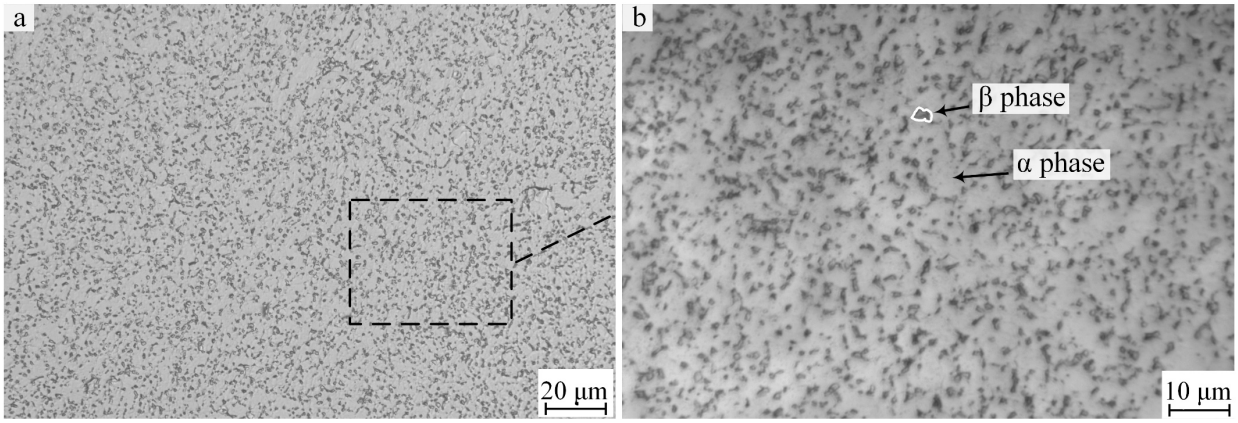

Fig. 1. Microstructure of the wrought Ti6Al4V in the as-received condition: 500x (a), and 1000x magnification (b).

Besides the arithmetic mean height *Sa*, the reduced valley height *Svk*, kurtosis *Sku,* and skewness *Ssk* were evaluated as surface texture parameters correlated to the metals' fatigue strength [8].

The FEI Quanta™ 450 scanning electron microscope (SEM) was used to inspect the severe plastic deformation (SPD) layer beneath the machined surface at the minimum diameter of the specimen gauge length. To do that, samples were metallographically prepared using the procedure above described, and the SPD layer extent was evaluated every 5 µm from the surface.

Residual stresses at the minimum diameter of the specimen gauge length were evaluated making use of a SpiderX™ GNR portable instrument equipped with a hybrid photon counting detector till a distance of 150 µm from the machined surface. To do that, a layer of material was removed after each acquisition by electropolishing in a solution consisting of 90 ml water, 730 ml ethanol, 100 ml butoxyethanol, and 78 ml perchloric acid.

Fatigue tests were carried out on a Metro Com™ machine adopting a four-point rotating bending configuration. Such configuration was chosen as it permits the evaluation of the actual influence of the cutting parameters on the material fatigue strength, being the specimen's outer region the most stressed. The runout criterion was fixed at 10^7 cycles according to literature studies dealing with Ti6Al4V fatigue strength [7]. The specimens were tested using a load ratio R=-1 until their complete separation, which was recorded as the number of cycles to failure N_f.

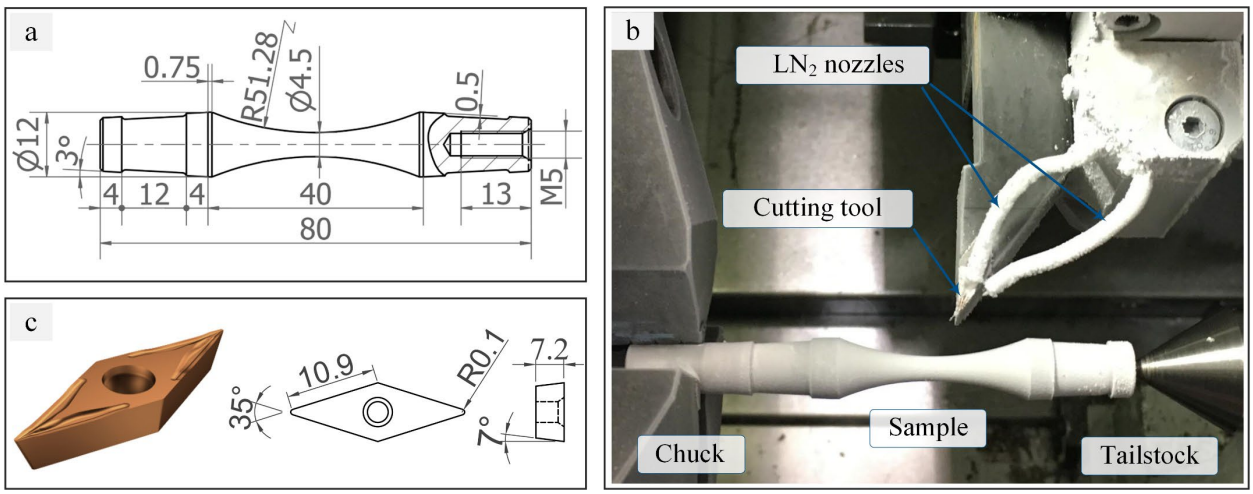

Fig. 2. Geometry of the specimen for fatigue testing (a), machining set-up employing cryogenic cooling (b), geometry of the cutting tool (c).

The fatigue limit was determined using the staircase method according to ISO 12107 standard. SEM observations were carried out on the fatigue-fractured surfaces to identify the crack initiation location.

Results and discussion

Representative surface topographies of the Ti6Al4V specimens machined adopting flood and cryogenic lubricating-cooling conditions are shown in Fig. 3. It can be noted that the cryogenic machined specimen is characterized by a more irregular surface than the flood machined one. Although the same cutting parameters were used, the latter is characterized by more visible, marked, and regular grooves due to the passage of the tool during turning, in accordance with other literature records on cryogenic machining [9].

The differences between the two sets of specimens in terms of surface quality can be more appreciated from the roughness profiles extracted from the above-shown surface topographies and reported in Fig. 4a and Fig. 4b. The corresponding areal parameters are shown in Fig. 4c and reported in Table 1, where the percentage difference (Δ%) between the flood and cryogenic machined specimens is also highlighted.

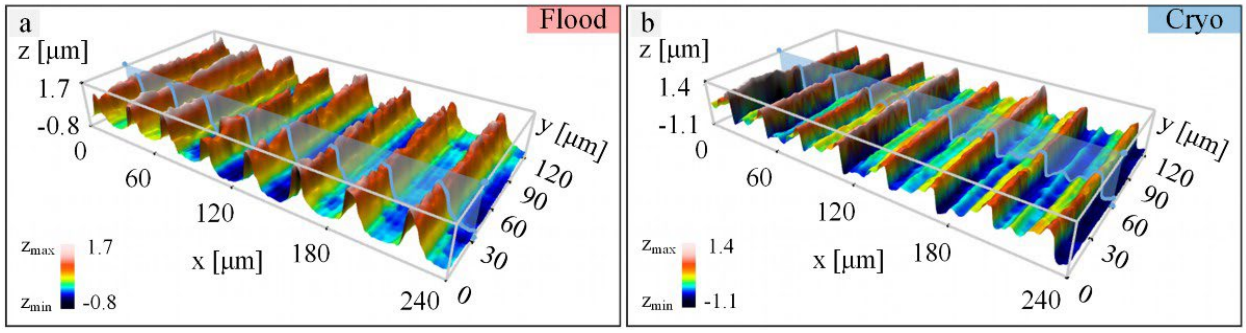

Fig. 3. Representative surface topography of specimens machined using flood lubrication (a), and cryogenic cooling (b).

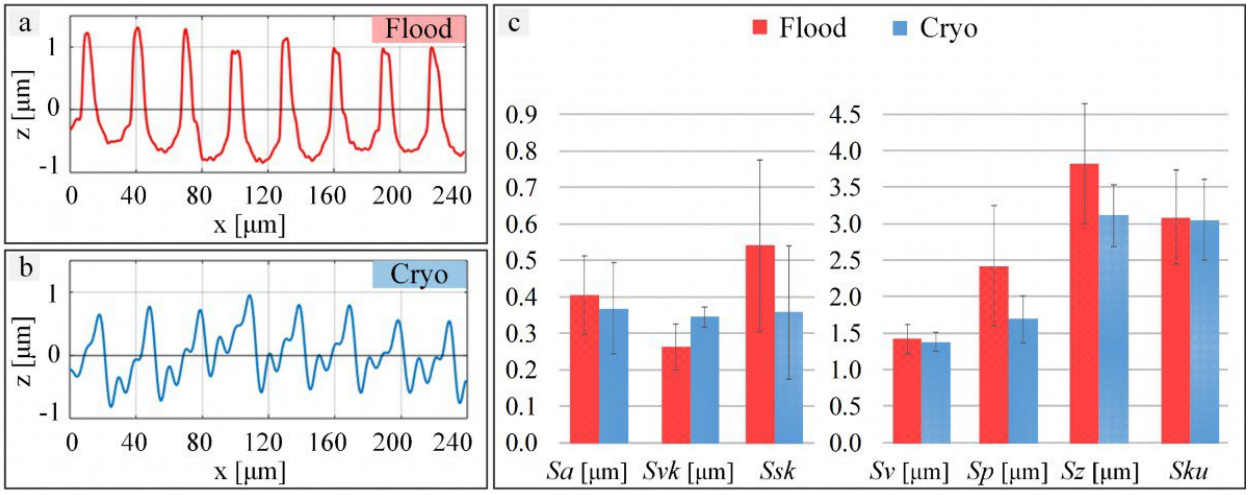

Fig. 4. Representative roughness profiles of the flood (a) and cryogenic (b) machined specimens; surface roughness parameters at varying lubricating-cooling conditions (c).

Materials Research Proceedings 41 (2024) 1935-1944 https://doi.org/10.21741/9781644903131-214

Table 1. Surface roughness parameters at varying lubricating-cooling conditions.

Conditions	*Sa* [μm]	*Svk* [μm]	*Sv* [μm]	*Sp* [μm]	*Sz* [μm]	*Ssk*	*Sku*
Flood	0.40±0.10	0.26±0.06	1.40±0.19	2.40±0.82	3.80±0.81	0.54±0.23	3.13±0.65
Cryo	0.36±0.12	0.34±0.03	1.36±0.13	1.68±0.31	3.10±0.42	0.36±0.18	3.09±0.55
Δ %	-9%	31%	-3%	-30%	-18%	-33%	-1%

The quality of a machined surface is generally assessed through the average roughness *Sa*: the cryogenic machined specimens are characterized by *Sa* 9% lower than the one of the flood machined specimens, however, the standard deviation of the measured values does not allow assessing a statistically significant difference. When addressing fatigue phenomena, the *Sv* parameter, which represents the maximum pit depth, is particularly relevant because the valleys of the roughness profile can be considered as possible crack initiation sites. Nevertheless, both the flood and cryogenic machined samples show nearly the same *Sv* values. The cryogenic machined specimens present a surface characterized by a maximum roughness height *Sz* 18% lower than the one of the flood machined specimens, which should indicate better fatigue life of the cryogenic machined samples than the flood ones. More precisely, the difference in terms of *Sz*, which is defined as the sum of the largest peak height value and the largest pit depth value, in this case, is due to a significant reduction in the peak heights for the cryogenic samples. The latter shows the maximum peak height parameter *Sp* 30% lower than the flood one while maintaining the same *Sv*.

The value of *Ssk* (skewness) gives information about the asymmetry of the distribution of the material, in terms of peaks and valleys, on the surface. In particular, if $Ssk < 0$ there is a predominance of valleys, whereas if $Ssk > 0$ there is a predominance of peaks. If $Ssk > 0$, this means that the material is close to the valleys on the surface. Both the flood and cryogenic machined samples have $Ssk > 0$, namely a predominance of peaks, which is positive for the fatigue life.

The kurtosis *Sku* is a measure of the sharpness of the surface roughness and indicates the presence of excessive peaks and valleys if $Sku > 3$ or their absence on the surface if $Sku < 3$. A normal height distribution, so that sharp portions and indented portions coexist, is characterized by $Sku = 3$. Negative skewness with a predominance of valleys has an adverse effect on fatigue [8], while high kurtosis determines the presence of sharp peaks or valleys. Both the flood and cryogenic machined samples show a positive kurtosis.

Even if both sets of specimens exhibit *Sku* close to 3, however, the cryogenic machined specimens are characterized by more irregular valleys, which is evident from a higher *Svk* reduced valley height and lower skewness. The *Svk* parameter measures the depth of the valleys below the core roughness and is generally considered important in functional surface characteristics, such as lubrication, as a lubricant can pool in these small valleys and provide greater wear resistance. High *Svk* may indicate a higher number of crack initiation sites and crack propagation, however, the most influential parameter regarding fatigue life is the total height of the valleys, *Sv,* along with *Ssk* and *Sku*, which define or not the dominance of valleys and how acute these are [10]. Overall, the analysis of the surface topographies cannot lead to the conclusion that one surface is better than the other in terms of texture parameters correlated to fatigue life.

As it is well known, machining operations tend to form a severe plastic deformation (SPD) layer just below the machined surface. This is due to the large localized deformation that occurs at the shearing plane during chip formation.

Fig. 5 shows two SEM images obtained with the backscattered electron detector, highlighting the SPD layers developed when machining using flood and cryogenic cooling conditions.

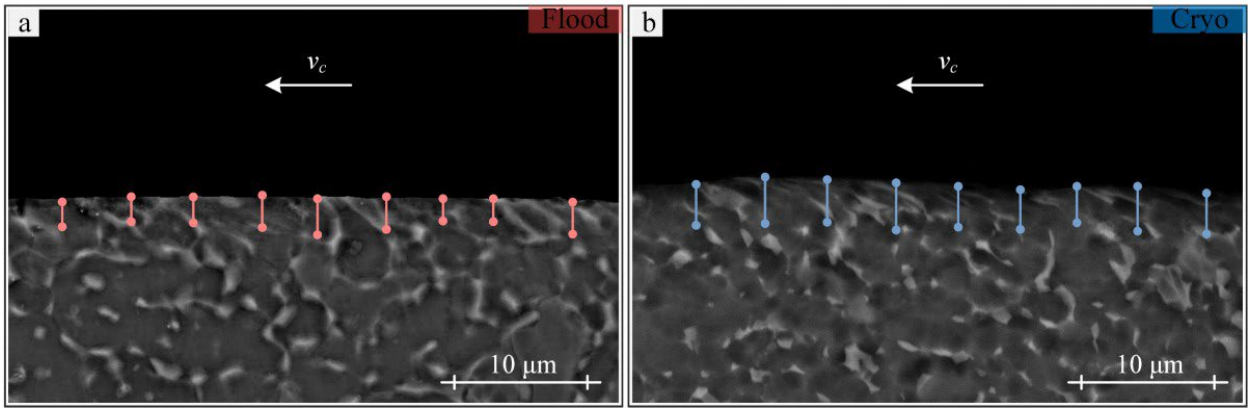

Fig. 5. Microstructure below the machined surface and highlight of SPD layer below the surface of the flood (a) and cryogenic (b) machined specimens.

The SPD layer thickness was determined using 9 measurements per specimen type, spaced about 5 µm, as can be seen in Fig. 5. The samples obtained by turning with liquid nitrogen show considerable deformation of the grains close to the machined surface: in particular very elongated β grains can be observed along the cutting speed direction, in contrast to the bulk material, which has equiaxed grains. The layer affected by this remarkable deformation has a thickness of 3.61 ± 0.28 µm. In contrast, the flood machined specimens show less evident grain deformation along with a smaller thickness of the SPD layer, namely 2.50 ± 0.40 µm. The SPD layer observed after cryogenic machining is 44% higher than the one after flood machining, following other literature studies [11, 12]. The plastic deformations induced by machining, in addition to being visible in the thickness of the SPD layer, introduce constraints within the material that create a field of self-compensating stresses known as residual stresses. During the life of a mechanical component, residual stresses combine with applied external loads and can have both positive and negative effects. Residual stresses also influence the component's mechanical properties as well as its corrosion resistance [13, 14]. Compressive residual stresses are desirable as they generally have beneficial effects [15] in terms of fatigue resistance, especially when the component is subjected to high surface stresses during its service life. The residual stresses of the post-machined specimens along the axial direction $\sigma_{r,zz}$ were analyzed using X-ray diffraction, and are reported in the diagram of Fig. 6 as a function of the distance *d* from the machined surface. The residual stresses along the axial direction are here considered as the ones influencing the fatigue life of components whose surface is subjected to tension or bending, as in the case of this study. For better sake of comparison, the residual stress values under flood and cryogenic cooling conditions are also given in Table 2.

Table 2. Axial residual stresses of the flood and cryogenic machined specimens.

Flood		Cryo	
d [µm]	$\sigma_{r,zz}$ [MPa]	*d* [µm]	$\sigma_{r,zz}$ [MPa]
0 ± 0	-492 ± 25	0 ± 0	-964 ± 27
9 ± 3	-214 ± 14	7 ± 2	-519 ± 16
23 ± 3	43 ± 13	43 ± 1	24 ± 12
30 ± 2	39 ± 8	52 ± 2	72 ± 14
85 ± 2	146 ± 12	79 ± 2	120 ± 11
140 ± 2	17 ± 12	150 ± 3	67 ± 12

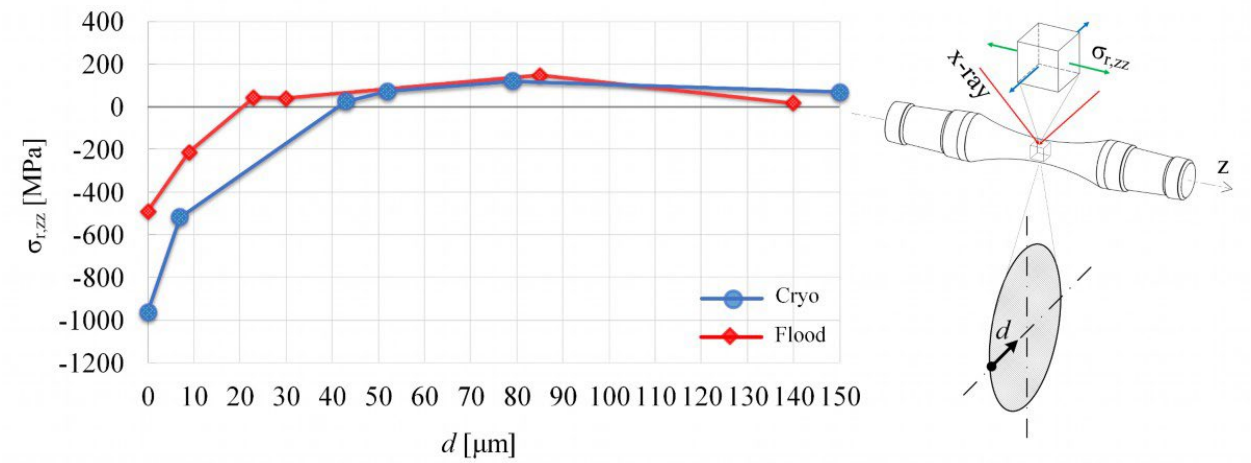

Fig. 6. Axial residual stresses of flood and cryogenic machined specimens as a function of distance from the machined surface (see Table 2 for the standard deviations data).

The cryogenic machined specimens are characterized by remarkable residual compressive surface stresses, namely $\sigma_{r,zz}$ = -964 ± 27 MPa, whereas the conventionally machined specimens have a compressive surface stress that is about 51% lower, namely $\sigma r,_{zz}$ = -492 ± 25 MPa. The residual stress state of the cryogenic machined samples tends to disappear less rapidly than that of the flood machined samples, reaching 0 MPa within 40 µm of the surface under cryogenic cooling and 30 µm under flood one. The stresses gradient observed from the external surface to the bulk material is very high compared to what is usually found in the literature on additive manufactured Ti6Al4V specimens with lamellar microstructure processed by turning, nevertheless in the latter case the distances interested by the residual stress state are greater [5]. This is due to the particularly fine equiaxial microstructure that characterizes the specimens under consideration. The results in terms of axial residual stress of cryogenic and flood machined specimens are in accordance with the previous SPD layer measurements, highlighting the increased plastic deformation in cryogenic machining.

The four-point rotating bending test configuration was selected to determine fatigue curves because it ensures the highest stress intensity on the annular outer layers of the specimens, highlighting the effects of machining, surface integrity, and residual stresses. The tests were conducted using a load ratio R = -1, which is defined as the ratio between the minimum and maximum stress. Fig. 7a displays the experimental data and fatigue curves processed using the nominal stress approach with a 50% survival probability (SP), i.e. the Wöhler curve. The data are presented in terms of nominal stress amplitude (σ_a) versus cycles to failure (N_f).

The fatigue limit (σ_A), which is the stress amplitude for which a cyclically stressed specimen exhibits infinite life, was calculated using the modified staircase method, by using Eq. 1 where *i* is the *i*-th specimen in the test sequence using a σ_i stress level and *n* is the number of effectively tested specimens. It is worth underlining that the first stress level is not counted in Eq. 1 because it is a non-statistical datum affected by the operator's choice. The adopted test sequences and the number *n* of effectively tested specimens (7 for flood and 6 for cryogenic) are shown in Table 3, where a 25 MPa stress step was assumed according to ISO 12107, which requires the use of at least 6 specimens for the application of Eq. 1.

$$\sigma_A = \frac{1}{n}\sum_{i=2}^{n+1}\sigma_i \tag{1}$$

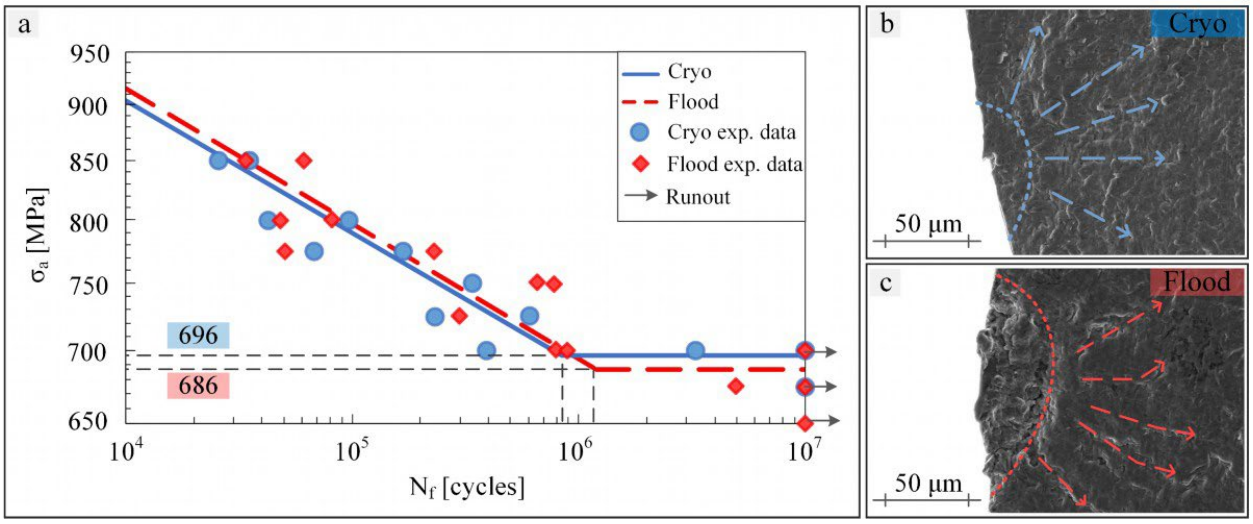

Fig. 7. Fatigue test data of Ti6Al4V wrought specimens in terms of nominal stress amplitude at varying machining cooling strategies (a), crack initiation zone at the fatigue fracture surface in the cryogenic (b) and flood conditions (c).

Table 3. Modified staircase test data

Flood	Stress sequence (σ_i) [MPa]	700	675	700	725	700	675	650	675
	Event	X*	O	O	X	X	X	O	a
Cryo	Stress sequence (σ_i) [MPa]	725	700	725	700	675	700	675	
	Event	X*	O	X	X	O	X	a	

X: failure, O: no failure, a: not actually carried out (calculated from previous value), * not counted

The fatigue limit was found to be 686 MPa and 696 MPa for the flood and cryogenic cryo machined series, respectively (see Fig. 7a). The knee of the Wöhler curve was not imposed for a certain number of cycles, but it was determined as the intersection of the calculated fatigue limit and the fatigue curve at SP 50%, as reported in Table 4. The inverse slope (k) of the fatigue curve for the cryogenic machined specimens is only 2% higher than that of the flood machined ones, meaning that there are no appreciable differences in the high-cycle fatigue range below 10^6 cycles (see Table 4). The scatter index $T_{\sigma,10\text{-}90\%}$, which is defined as the ratio between the fatigue strength at 10% SP and 90% SP at a given number of cycles, is 1.22 and 1.16 for the flood and cryogenic machined, respectively. The scatter index is perfectly comparable between the two series of specimens.
There is only a difference of 5%, which can be considered negligible. Furthermore, values lower than 1.6 are normally acceptable and indicate good repeatability between the results and low statistical deviation.

Table 4. Fatigue data of the flood and cryogenic machined specimens.

Conditions	R	# data	# runout	σ_A [MPa]	N_A	*k*	$T_{\sigma,10\text{-}90\%}$
Flood	-1	17	5	686	$1.2 \cdot 10^6$	16.60	1.22
Cyo	-1	15	4	696	$8.5 \cdot 10^5$	16.94	1.12

The fatigue ratio (R_f) is the ratio between the fatigue limit and UTS. R_f is typically around 0.5 for many metals, including steels and titanium alloys. However, in the case of titanium alloys as is Ti6Al4V, R_f can vary significantly depending on the microstructure and grain size [7, 16]. In the conducted tests, the fatigue ratio was approximately 0.7 for both flood and cryogenic machined specimens. This indicates that the material has high fatigue strength, regardless of the

strategy used to machine it, which can be ascribed to its fine equiaxial microstructure. This is in accordance with literature records, where Ti6Al4V, even if processed with other methods than the one of this study, with a fine equiaxial microstructure was characterized by higher fatigue strength compared to the same alloy but with coarse equiaxial or lamellar microstructures [1, 7].

Finally, the graph in Fig. 7a shows a difference of only 10 MPa between the two cutting conditions at the fatigue limit, around 10^6 cycles. This difference can be attributed to the higher and deeper compressive residual stresses found in the cryogenic machined specimens. The effect of these stresses is not noticeable for a lower number of cycles where the phenomenon of residual stress relaxation occurs [14, 17].

After conducting the fatigue tests, the specimen fracture surfaces were analyzed and the crack initiation zones were identified (see Fig. 7b and 7c). No internal or sub-surface defects from which the crack could originate were found, meaning that the mechanism of initiation, propagation, and static fracture is the same for both the sets of specimens, namely the fatigue fracture starts from the valleys of the roughness profile, the latter being likely crack initiation sites.

Conclusions

Ti6Al4V wrought specimens, characterized by an equiaxed α phase and intergranular β phase, with an average grain size of 2.6 ± 0.3 μm, were machined with two different lubricating-cooling strategies, i.e. cryogenic and flood. The surface integrity of the machined specimens was evaluated focusing on the fatigue-related roughness parameter, the SPD layer thickness, and axial residual stresses. Fatigue tests were conducted using a rotating bending load configuration and fatigue strength was derived. This study evaluates the fatigue strength of a wrought Ti6Al4V provided with a very fine microstructure and machined under flood and cryogenic cooling conditions. The following conclusions can be drawn:

- The average roughness of the flood and cryogenic machined specimens is very similar, whereas other surface texture parameters that are usually correlated to metal fatigue life do not provide a definitive answer about the likeliness of higher fatigue strength of any of the two sets of specimens.
- Cryogenic machined specimens show higher and deeper compressive residual stresses as well as higher SPD layers than flood-machined ones.
- The fatigue limit of the two sets of specimens is nearly the same, with fatigue fracture always starting from the valleys of the roughness profile. This very similar behavior in terms of fatigue strength can be ascribed to the very fine microstructure characterizing the wrought alloy in its as-received condition, which prevails over the other characteristics induced by any machining strategy.

References

[1] C. Leyens, & M. Peters (Eds.), Titanium and titanium alloys: fundamentals and applications, Wiley-vch (2006).

[2] M. O. Bodunrin, L. H. Chown, J. W. van der Merwe, K. K. Alaneme, Hot working of Ti-6Al-4V with a complex initial microstructure, International Journal of Material Forming (2019), 12, pp. 857-874.

[3] Y. Yildiz, & M. Nalbant, A review of cryogenic cooling in machining processes, International Journal of Machine Tools and Manufacture (2008), 48(9), 947-964.

[4] D. Umbrello, & G. Rotella, Fatigue life of machined Ti6Al4V alloy under different cooling conditions, CIRP Annals (2018), 67(1), 99-102. https://doi.org/10.1016/j.cirp.2018.03.017

[5] R. Bertolini, A. Campagnolo, M. Sorgato, A. Ghiotti, S. Bruschi, & G. Meneghetti, Fatigue strength of LPBF Ti6Al4V machined under flood and cryogenic lubri-cooling conditions, International Journal of Fatigue (2022), 162, 106973. https://doi.org/10.1016/j.ijfatigue.2022.106973

[6] A. Ghiotti, R. Bertolini, M. Sorgato, A. Campagnolo, E. Savio, & S. Bruschi, Ti6Al4V titanium alloy fatigue strength after AM-and machining-based process chains, CIRP Annals (2022), 71(1), 461-464. https://doi.org/10.1016/j.cirp.2022.04.021

[7] G. Lütjering, J.C. Williams, Titanium, Springer (2007).

[8] M. Dumas, F. Cabanettes, R. Kaminski, F. Valiorgue, E. Picot, F. Lefebvre, & J. Rech Influence of the finish cutting operations on the fatigue performance of Ti-6Al-4V parts produced by Selective Laser Melting, Procedia CIRP (2018), 71, 429-434. https://doi.org/10.1016/j.procir.2018.05.054

[9] S. Sartori, A. Bordin, A. Ghiotti, S. Bruschi, Analysis of the surface integrity in cryogenic turning of Ti6Al4V produced by Direct Melting Laser Sintering, procedia CIRP (2016), 45 123-126. https://doi.org/10.1016/j.procir.2016.02.328

[10] S. Lee, B. Rasoolian, D. F. Silva, J. W. Pegues, N. Shamsaei, Surface roughness parameter and modeling for fatigue behavior of additive manufactured parts: a non-destructive data-driven approach, Addit Manuf (2021), 46, 10209. https://doi.org/10.1016/j.addma.2021.102094

[11] Y. Sun, B. Huang, D. A. Puleo, J. Schoop, & I. S. Jawahir, Improved surface integrity from cryogenic machining of Ti-6Al-7Nb alloy for biomedical applications, Procedia Cirp (2016), 45, 63-66. https://doi.org/10.1016/j.procir.2016.02.362

[12] G. Rotella, O. W. Dillon, D. Umbrello, L. Settineri, & I. S. Jawahir, The effects of cooling conditions on surface integrity in machining of Ti6Al4V alloy, The International Journal of Advanced Manufacturing Technology (2014), 71, 47-55. https://doi.org/10.1007/s00170-013-5477-9

[13] R. Bertolini, S. Bruschi, A. Bordin, A. Ghiotti, L. Pezzato, M. Dabalà, Fretting Corrosion Behavior of Additive Manufactured and Cryogenic-Machined Ti6Al4V for Biomedical Applications, Advanced Engineering Materials (2016), 19(6), 1500629.

[14] R. W. Landgraf, & R. A. Chernenkoff, Residual stress effects on fatigue of surface processed steels. Analytical and experimental methods for residual stress effects in fatigue, ASTM STP (1988), 1004, 1-12.

[15] G. S. Schajer, (Ed.), Practical residual stress measurement methods. John Wiley & Sons (2013).

[16] Y. Murakami, Metal fatigue: effects of small defects and nonmetallic inclusions, Elsevier (2019).

[17] R. C. McClung, A literature survey on the stability and significance of residual stresses during fatigue, Fatigue & Fracture of Engineering Materials & Structures (2007), 30(3), 173-205.